



Transit cosmological models in $F(R, \bar{T})$ gravity theory

Dinesh Chandra Maurya^{1,a} , Ratbay Myrzakulov^{2,b}

¹ Centre for Cosmology, Astrophysics and Space Science, GLA University, Mathura, Uttar Pradesh 281 406, India

² Eurasian International Centre for Theoretical Physics and Department of General and Theoretical Physics, Eurasian National University, 010008 Astana, Kazakhstan

Received: 1 January 2024 / Accepted: 13 May 2024 / Published online: 28 May 2024
© The Author(s) 2024

Abstract In the present paper, we investigate some exact cosmological models in $F(R, \bar{T})$ gravity theory. We have considered the arbitrary function $F(R, \bar{T}) = R + \lambda \bar{T}$ where λ is an arbitrary constant, R, \bar{T} are respectively, the Ricci-scalar curvature and the torsion. We have solved the field equations in a flat FLRW spacetime manifold for Hubble parameter and using the MCMC analysis, we have estimated the best fit values of model parameters with $1 - \sigma, 2 - \sigma, 3 - \sigma$ regions, for two observational datasets like $H(z)$ and Pantheon SNe Ia datasets. Using these best fit values of model parameters, we have done the result analysis and discussion of the model. We have found a transit phase decelerating-accelerating universe model with transition redshifts $z_t = 0.4438^{+0.1008}_{-0.0790}, 0.3651^{+0.1644}_{-0.0904}$. The effective dark energy equation of state varies as $-1 \leq \omega_{de} \leq -0.5176$ and the present age of the universe is found as $t_0 = 13.8486^{+0.1005}_{-0.0640}, 12.0135^{+0.6206}_{-0.2743}$ Gyrs, respectively for two datasets.

1 Introduction

The universe underwent two episodes of accelerated expansion at early and late times of the cosmological evolution, according to the conventional paradigm of cosmology, which is based on a growing amount of observable data. Although the cosmological constant might be the best explanation for the late-time acceleration, the possibility that the acceleration is dynamic in nature and the presence of some potential tensions may call for a revision of our understanding—something that is unquestionably necessary for early time acceleration. There are primarily two paths one could take in order to accomplish this. The first is to build extended gravitational theories that, although having general relativity as a specific limit, can generally offer more degrees of freedom to adequately describe the evolution of the universe [1,2]. The second approach is to modify the conventional particle physics model and take general relativity into account. This involves assuming that the universe contains additional matter in the form of dark energy [3,4] and/or inflation fields [5]. Keep in mind that the first approach has the extra theoretical benefit of may be leading to an improved [6,7].

One can begin building gravitational modifications from the Einstein-Hilbert action, that is, from the curvature description of gravity, and extend it appropriately, as in the cases of Lovelock gravity [8,9], $F(R)$ gravity [10], and $F(G)$ gravity [11,12]. He may also examine torsional modified gravities, such as $F(T)$ gravity [13–15], $F(T, T_G)$ gravity [16], etc., starting with the analogous, teleparallel formulation of gravity in terms of torsion [17,18]. Cosmologists are interested in $f(T)$ teleparallel gravity, one of the intriguing modified theories of gravity. The study of modified Teleparallel $f(T)$ gravity, where T is the torsion scalar, was driven by the generalization of $f(R)$ gravity, where R is the Ricci scalar. To characterize the effects of gravitation in terms of torsion rather than curvature, [19–22] employed the curva-

Contents

1 Introduction	1
2 $F(R, \bar{T})$ gravity and field equations	2
3 Cosmological solutions for $F(R, \bar{T}) = R + \lambda \bar{T}$	3
4 Observational constraints	4
4.1 Hubble function	4
4.2 Apparent magnitude $m(z)$	6
5 Result analysis and discussion	7
5.1 Om diagnostic analysis	10
5.2 Age of the universe	10
5.3 Information criteria	11
6 Conclusions	11
References	12

^ae-mail: dcmaurya563@gmail.com (corresponding author)

^be-mail: rmyrzakulov@gmail.com

tureless Weitzenböck connection in teleparallel gravity, as opposed to the traditional torsionless Levi–Civita connection in general relativity.

The linear forms of $f(T)$ lead to a teleparallel gravity equivalent to general relativity (TEGR) [23]. Nonetheless, there are disparities in the physical interpretations of the two theories of gravity, $f(T)$ and $f(R)$. In $f(T)$ gravity, the torsion scalar T just comprises the first-order derivatives of the vierbeins, but in $f(R)$ gravity, the second-order derivatives of the metric tensor are contained in the Ricci scalar R . This means that, as opposed to other modified theories of gravity, the exact solutions of cosmological models in $f(T)$ gravity may be readily found. $f(T)$ gravity is a straightforward modified theory of gravity, however there aren't many precise solutions suggested in the literature. In isotropic and anisotropic spacetime, some cosmological models [24–26] with power-law solutions have been discovered in the literature. Some cosmologists have studied some exact solutions of the cosmological models in [19, 27, 28] for static spherically symmetric spacetime and Bianchi type-I spacetime. When compared to other modified theories of gravity, the analysis of cosmic situations in $f(T)$ gravity is straightforward. Consequently, a large number of cosmological scenarios, including the big bounce [29–32], inflationary model [33], and late time cosmic acceleration [34–36], are studied using $f(T)$ gravity theory. In the field of $f(T)$ gravity, there have been recent developments including spherical and cylindrical solutions [37], conformally symmetric traversable wormholes [38], and noether charge and black hole entropy [39]. Recently, we have discussed and reconstructed some Λ CDM cosmological models in $f(T)$ gravity [40–43].

Additionally, nonmetricity could be used to create gravitational alterations [44]. Furthermore, altering the fundamental geometry itself might give rise to an intriguing class of modified gravity; this could include, for example, Finsler or Finsler-like geometries [45–48]. The non-linear connection's potential to introduce additional degrees of freedom and make the gravitational modification phenomenologically interesting is one of the framework's intriguing features [49, 50]. This feature was also obtained through the use of a different theoretical framework for metric-affine theories [51–55].

In [56], R. Myrzakulov found an intriguing gravitational modification called the $F(R, \bar{T})$ gravity. Both curvature and torsion are dynamical fields associated with gravity in this theory because one makes use of a particular but non-special connection. Because of this, the theory has additional degrees of freedom originating from both the non-special connection and the arbitrary function in the Lagrangian. The theory belongs to the class of Riemann–Cartan theories, which are part of the broader category of metric theories with affine connections [57, 58]. A few of the theory's applications were examined in [56, 59–62]. Specifically, [56] addressed

certain theoretical concerns; [59] examined energy conditions; [60] examined theoretical relationships with various scenarios; [61] examined Noether symmetries; and [62] examined neutron star theory. Recently, in [63] have analyzed the resultant cosmology of such a framework and to compute the evolution of observable quantities like the effective dark energy equation-of-state parameter and density parameters. By expressing the theory as a deformation from both general relativity and its teleparallel counterpart, they have examined the cosmological behavior with an emphasis on the connection's effect by employing the mini-super-space approach. The observational constraints on $F(R, \bar{T})$ -gravity have been investigated in [64]. Various Metric-Affine Gravity Theories and its applications are discussed in [65–71].

Motivated by the above discussions, in this paper, we investigate a spatially flat, isotropic and homogeneous spacetime universe in $F(R, \bar{T})$ Gravity in the context of generalized connection Γ , in which curvature R and torsion T both are non-zero. The paper is organized as follows. In Sect. 2, we give a brief review of the $F(R, \bar{T})$ gravity theory. The cosmological solution for the particular linear case $F(R, \bar{T}) = R + \lambda \bar{T}$ are given in Sect. 3. Observational constraints for the model are studied in Sect. 4. The result analysis and discussions are presented in Sect. 5. The age of the universe is considered in Sect. 5.2. The last Sect. 6 is devoted to conclusions.

2 $F(R, \bar{T})$ gravity and field equations

To explore the cosmological properties of the universe in $F(R, \bar{T})$ gravity, we consider the flat Friedmann-Lemaître-Robertson-Walker (FLRW) space-time described by the metric

$$ds^2 = -dt^2 + a^2(t)(dx^2 + dy^2 + dz^2), \quad (1)$$

where $a = a(t)$ is the scale factor. The orthonormal tetrad components $e_i(x^\mu)$ are related to the metric through

$$g_{\mu\nu} = \eta_{ij} e_\mu^i e_\nu^j, \quad (2)$$

where the Latin indices i, j run over 0...3 for the tangent space of the manifold, while the Greek letters μ, ν are the coordinate indices on the manifold, also running over 0...3. We consider the action for $F(R, \bar{T})$ gravity [56, 63] as

$$S = \int e [F(R, \bar{T}) + L_m] dx^4, \quad (3)$$

where $e = \sqrt{-g}$ with g as the determinant of metric tensor $g_{\mu\nu}$, $R = R^{(LC)} + u$ and $\bar{T} = \bar{T}^{(W)} + v$ with $R^{(LC)}$ is the Ricci scalar corresponding to Levi–Civita connection and $\bar{T}^{(W)}$ is the torsion scalar corresponding to Weitzenböck connection. And u is a scalar quantity depending on the tetrad, its first and second derivatives, and the connection and its first derivative,

and v is a scalar quantity depending on the tetrad, its first derivative and the connection. Hence, u and v quantify the information on the specific imposed connection [63].

The general modified field equations for $F(R, \bar{T})$ gravity are obtained by varying the action (3) with respect to metric field as below (see the reference [65] for detail):

$$F_R R_{(\mu\nu)} - \frac{1}{2}g_{\mu\nu}F + F_{\bar{T}} \times \left(2S_{vij}S_{\mu}^{ij} - S_{ij\mu}S^{ij}{}_{\nu} + 2S_{vij}S_{\mu}^{ji} - 4S_{\mu}S_{\nu} \right) = T_{\mu\nu} \tag{4}$$

where $F_R = \frac{\partial F}{\partial R}$, $F_{\bar{T}} = \frac{\partial F}{\partial \bar{T}}$, $R_{(\mu\nu)}$ is the symmetric part of the Ricci tensor of the affine connection Γ , $S_{\mu\nu}{}^{\lambda}$ is the torsion tensor, S_{μ} is the torsion trace, T_{ij} is the stress-energy momentum tensor defined by

$$T_{\mu\nu} = -\frac{2}{\sqrt{-g}} \frac{\delta(\sqrt{-g}L_m)}{\delta g^{\mu\nu}} \tag{5}$$

On the other hand, the connection field equations are

$$P_{\lambda}{}^{\mu\nu}(F_R) + 2F_{\bar{T}} \left(S^{\mu\nu}{}_{\lambda} - 2S_{\lambda}{}^{[\mu\nu]} - 4S^{[\mu}{}_{\lambda}{}^{\nu]} \right) = 0 \tag{6}$$

where $P_{\lambda}{}^{\mu\nu}(F_R)$ is the modified Palatini tensor,

$$P_{\lambda}{}^{\mu\nu}(F_R) = -\frac{\nabla_{\lambda}(\sqrt{-g}F_R g^{\mu\nu})}{\sqrt{-g}} + \frac{\nabla_{\alpha}(\sqrt{-g}F_R g^{\mu i} \delta_{\lambda}^{\nu})}{\sqrt{-g}} + 2F_R(S_{\lambda} g^{\mu\nu} - S^{\mu} \delta_{\lambda}^{\nu} - S_{\lambda}{}^{\mu\nu}) \tag{7}$$

with ∇ as the covariant derivative associated with the general affine connection Γ .

Here, we consider the energy momentum tensor for perfect fluid matter source as

$$T_{\mu\nu} = (\rho + p)U_{\mu}U_{\nu} + pg_{\mu\nu} \tag{8}$$

where ρ , p are respectively, energy density and pressure of the considered perfect fluid matter source, $U^{\mu} = (-1, 0, 0, 0)$ is the four velocity vector.

In this paper, we restrict ourselves to the case $u = u(a, \dot{a})$ and $v = v(a, \dot{a})$. The scale factor $a(t)$, the curvature scalar R and the torsion scalar \bar{T} are taken as independent dynamical variables. Then after some algebra the action (3) becomes [72],

$$S = \int L dt, \tag{9}$$

where the point-like Lagrangian is given by

$$L = a^3(F - \bar{T}F_{\bar{T}} - RF_R + vF_{\bar{T}} + uF_R) - 6(F_R + F_{\bar{T}})a\dot{a}^2 - 6(F_{RR}\dot{R} + F_{R\bar{T}}\dot{\bar{T}})a^2\dot{a} - a^3L_m. \tag{10}$$

The corresponding field equations of $F(R, \bar{T})$ gravity are obtained in [72,73], as

$$3H\dot{R}F_{RR} - 3(\dot{H} + H^2)F_R + 3H\dot{\bar{T}}F_{R\bar{T}} + 6H^2F_{\bar{T}}$$

$$+ \frac{1}{2}F - \frac{1}{2}\dot{a}u_{\dot{a}}F_R - \frac{1}{2}\dot{a}v_{\dot{a}}F_{\bar{T}} = \rho, \tag{11}$$

$$\begin{aligned} & \dot{R}^2 F_{RRR} + (\ddot{R} + 2\dot{R}H)F_{RR} + (3H^2 + 2\dot{H} - \frac{1}{2}R) \\ & \times (F_R + F_{\bar{T}}) + 2\dot{\bar{T}}HF_{\bar{T}\bar{T}} + 2\dot{R}\dot{\bar{T}}F_{R\bar{T}} + \dot{\bar{T}}^2 F_{R\bar{T}\bar{T}} \\ & + (2\dot{R}H + 2\dot{\bar{T}}H + \ddot{\bar{T}})F_{R\bar{T}} + \frac{1}{2}F - \frac{1}{6}au_{\dot{a}}\dot{R}F_{RR} \\ & - (\frac{1}{2}\dot{a}u_{\dot{a}} + \frac{1}{6}a\dot{u}_{\dot{a}} - \frac{1}{2}u - \frac{1}{6}au_a)F_R \\ & - \frac{1}{6}av_{\dot{a}}\dot{\bar{T}}F_{\bar{T}\bar{T}} - (\frac{1}{2}\dot{a}v_{\dot{a}} + \frac{1}{6}a\dot{v}_{\dot{a}} - \frac{1}{2}v - \frac{1}{6}av_a)F_{\bar{T}} \\ & - \frac{1}{6}a(v_{\dot{a}}\dot{R} + u_{\dot{a}}\dot{\bar{T}})F_{R\bar{T}} = -p. \end{aligned} \tag{12}$$

where

$$\begin{aligned} \rho &= L_m - \dot{a} \frac{\partial L_m}{\partial \dot{a}}, \\ p &= \frac{1}{3a^2} \left[\frac{d}{dt} \left(a^3 \frac{\partial L_m}{\partial \dot{a}} \right) - \frac{\partial}{\partial a} (a^3 L_m) \right]. \end{aligned} \tag{13}$$

3 Cosmological solutions for $F(R, \bar{T}) = R + \lambda \bar{T}$

In this investigation, we take the arbitrary function $F(R, \bar{T})$ in linear form in R and \bar{T} as given by

$$F(R, \bar{T}) = R + \lambda \bar{T}, \tag{14}$$

where λ is an arbitrary constant, $R = u + 6(\dot{H} + 2H^2)$ and $\bar{T} = v - 6H^2$. Using Eq. (14) in Eqs. (11) and (12), we obtain the field equations in the form

$$3(1 + \lambda)H^2 + 0.5[(u - \dot{a}u_{\dot{a}}) + \lambda(v - \dot{a}v_{\dot{a}})] = \rho, \tag{15}$$

and

$$\begin{aligned} & (1 + \lambda)(2\dot{H} + 3H^2) + 0.5[u - \dot{a}u_{\dot{a}} - \frac{1}{3}a\dot{u}_{\dot{a}} \\ & + \frac{1}{3}au_a] + 0.5\lambda[v - \dot{a}v_{\dot{a}} - \frac{1}{3}a\dot{v}_{\dot{a}} + \frac{1}{3}av_a] = -p. \end{aligned} \tag{16}$$

The energy conservation equation is obtained as

$$\begin{aligned} \dot{\rho} + 3H(\rho + p) &= \frac{1}{2}(\dot{u} - \dot{a}u_{\dot{a}} - \ddot{u}u_{\dot{a}}) \\ &+ \frac{1}{2}\lambda(\dot{v} - \dot{a}v_{\dot{a}} - \ddot{v}v_{\dot{a}}) \end{aligned} \tag{17}$$

Now, we consider the scalars u and v in the form of [70]

$$u = c_1 \frac{\dot{a}}{a} \ln \dot{a}, \quad v = s(a)\dot{a}, \tag{18}$$

where c_1 is an arbitrary constant and $s(a)$ is an arbitrary function of scale factor a .

Using Eq. (18) in Eqs. (15)–(17), we get the following form of the field equations (15)–(17):

$$3(1 + \lambda)H^2 - \frac{1}{2}c_1H = \rho, \quad (19)$$

$$(1 + \lambda)(2\dot{H} + 3H^2) - \frac{1}{2}c_1H - \frac{1}{6}c_1\frac{\dot{H}}{H} = -p. \quad (20)$$

and

$$\dot{\rho} + 3H(\rho + p) = 0 \quad (21)$$

For $\lambda = 0$, $c_1 = 0$, the field equations, (19) and (20) will reduced into original Einstein's field equations in general relativity (GR). One can obtain the Friedmann like equations as

$$3H^2 = \rho + \rho_{MG}, \quad (22)$$

$$2\dot{H} + 3H^2 = -p - p_{MG}, \quad (23)$$

where ρ_{MG} , p_{MG} are the geometrical corrections in energy density and pressure, respectively given by

$$\rho_{MG} = \frac{1}{2}c_1H - 3\lambda H^2,$$

$$p_{MG} = -\left[\frac{1}{2}c_1H + \frac{1}{6}c_1\frac{\dot{H}}{H} - \lambda(2\dot{H} + 3H^2)\right]. \quad (24)$$

These, geometrical corrections, respectively, in energy density and pressure ρ_{MG} , p_{MG} , called as effective dark energy sector in $F(R, \bar{T})$ gravity. We can show that effective dark energy sector is conserved, namely $\dot{\rho}_{MG} + 3H(\rho_{MG} + p_{MG}) = 0$, and it can be easily deduced from matter energy conservation equation $\dot{\rho} + 3H(\rho + p) = 0$.

We define the matter equation of state as $p = \omega\rho$ with $\omega = \text{constant}$ and using Eqs. (19) and (20), we get

$$\frac{12(1 + \lambda)H - c_1}{6H}\dot{H} + \frac{6(1 + \lambda)H^2 - c_1H}{2}(1 + \omega) = 0, \quad (25)$$

or

$$\frac{12(1 + \lambda)H - c_1}{6(1 + \lambda)H^2 - c_1H}dH + 3(1 + \omega)\frac{da}{a} = 0. \quad (26)$$

After integration Eq. (26), we get

$$6(1 + \lambda)H^2 - c_1H - c_2\left(\frac{a_0}{a}\right)^{3(1+\omega)} = 0, \quad (27)$$

where c_2 is an integrating constant.

Solving Eq. (27) for Hubble parameter H , we obtain

$$H(a) = \frac{c_1}{12(1 + \lambda)} + \frac{1}{12} \times \sqrt{\left(\frac{c_1}{1 + \lambda}\right)^2 + \left(\frac{24c_2}{1 + \lambda}\right)\left(\frac{a_0}{a}\right)^{3(1+\omega)}}, \quad \lambda \neq -1. \quad (28)$$

For $c_1 = 0$, we get Hubble parameter as $H(a) = \frac{\sqrt{6c_2}}{6\sqrt{1+\lambda}}\left(\frac{a_0}{a}\right)^{3(1+\omega)/2}$ which gives a power-law expansion cosmology with a constant deceleration parameter (DP). If we take $c_2 = 0$, then we find $H = \text{constant}$ which gives exponential-law expansion cosmology with constant DP.

Using the relation $\frac{a_0}{a} = 1 + z$ [3], we get

$$H(z) = \frac{c_1}{12(1 + \lambda)} + \frac{1}{12} \sqrt{\left(\frac{c_1}{1 + \lambda}\right)^2 + \left(\frac{24c_2}{1 + \lambda}\right)(1 + z)^{3(1+\omega)}}, \quad \lambda \neq -1. \quad (29)$$

The deceleration parameter is derived from $q = -1 + (1 + z)\frac{H'}{H}$ as

$$q(z) = -1 + \frac{36(1 + \omega)c_2(1 + z)^{3(1+\omega)}}{\frac{c_1^2}{1+\lambda} + 24c_2(1 + z)^{3(1+\omega)} + c_1\sqrt{\left(\frac{c_1}{1+\lambda}\right)^2 + \frac{24c_2}{1+\lambda}(1 + z)^{3(1+\omega)}}}, \quad \lambda \neq -1. \quad (30)$$

4 Observational constraints

For our model and dataset combination, we use the freely available emcee program, available at [74], to conduct an MCMC (Monte Carlo Markov Chain) analysis so that we may compare the model with observational datasets. Through parameter value variation across a variety of cautious priors and analysis of the parameter space posteriors, the MCMC sampler constrains the model and cosmological parameters. We then obtain the one-dimensional and two-dimensional distributions for each parameter: the one-dimensional distribution represents the posterior distribution of the parameter, whilst the two-dimensional distribution shows the covariance between two different values.

4.1 Hubble function

To ensure the model's validity and feasibility, a model that aligns with observational datasets must be obtained. As a result, in order to obtain this condition, we first investigated 32 observed statistically non-correlated Hubble datasets $H(z)$ across redshift z , with $H(z)$ [75–82] having errors (see Table 1). We used the following χ^2 -test formula while fitting data:

$$\chi^2(c_1, c_2, \lambda, \omega) = \sum_{i=1}^{i=N} \frac{[(H_{ob})_i - (H_{th})_i]^2}{\sigma_i^2}$$

Where N denotes the total amount of data, H_{ob} , H_{th} , respectively, the observed and hypothesized datasets of $H(z)$ and standard deviations are displayed by σ_i .

Table 1 Observed values of $H(z)$

S. no.	z	$H(z)$	σ_H	References
1	0.07	69.0	19.6	[75]
2	0.09	69.0	12.0	[76]
3	0.12	68.6	26.2	[75]
4	0.17	83.0	8.0	[76]
5	0.179	75.0	4.0	[77]
6	0.199	75.0	5.0	[77]
7	0.2	72.9	29.6	[75]
8	0.27	77.0	14.0	[76]
9	0.28	88.8	36.6	[75]
10	0.352	83.0	14.0	[77]
11	0.3802	83.0	13.5	[78]
12	0.4	95.0	17.0	[76]
13	0.4004	77.0	10.2	[78]
14	0.4247	87.1	11.2	[78]
15	0.4497	92.8	12.9	[78]
16	0.47	89.0	50.0	[79]
17	0.4783	80.9	9.0	[78]
18	0.48	97.0	62.0	[80]
19	0.593	104.0	13.0	[77]
20	0.68	92.0	8.0	[77]
21	0.75	98.8	33.6	[81]
22	0.781	105.0	12.0	[77]
23	0.875	125.0	17.0	[77]
24	0.88	90.0	40.0	[80]
25	0.9	117.0	23.0	[76]
26	1.037	154.0	20.0	[77]
27	1.3	168.0	17.0	[76]
28	1.363	160.0	33.6	[82]
29	1.43	177.0	18.0	[76]
30	1.53	140.0	14.0	[76]
31	1.75	202.0	40.0	[76]
32	1.965	186.0	50.4	[82]

For Λ CDM model, we have considered the Hubble function $H(z) = H_0\sqrt{\Omega_{m0}(1+z)^3 + \Omega_{\Lambda0}}$ with $\Omega_{\Lambda0} = 1 - \Omega_{m0}$. Using this Hubble function, we have performed the MCMC analysis with 32 statistically non-correlated Hubble datasets $H(z)$ with error bars in $H(z)$. The output likelihood plots of H_0, Ω_{m0} at 68%, 95%, and 99% confidence levels are given in Fig. 1 and the best fit Hubble curve for Λ CDM model is shown in Fig. 3. We have obtained the best fit value of Hubble constant as $H_0 = 68.0^{+2.110}_{-2.137}$ km s⁻¹ Mpc⁻¹ by varying H_0 in the range $50 < H_0 < 100$ and Ω_{m0} in the range (0, 1) for Λ CDM model which is mentioned in Table 2.

The contour plots for model parameters c_1, c_2, λ , and ω at 68%, 95%, and 99% confidence levels, respectively, are shown in Fig. 2. The best fit shape of Hubble function

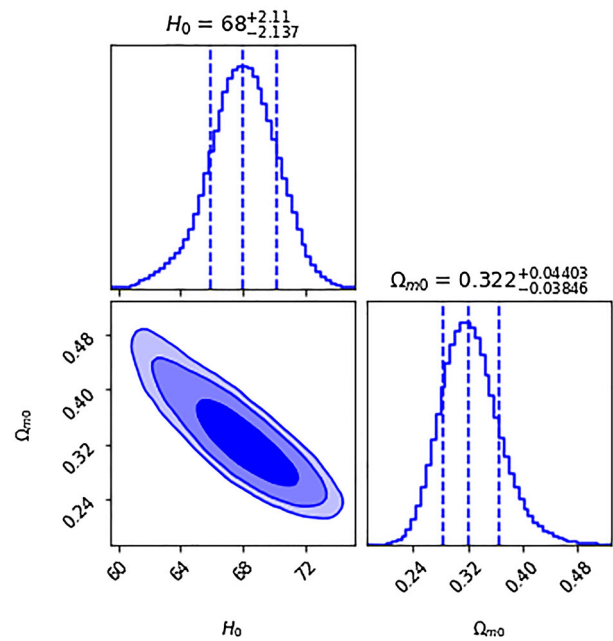


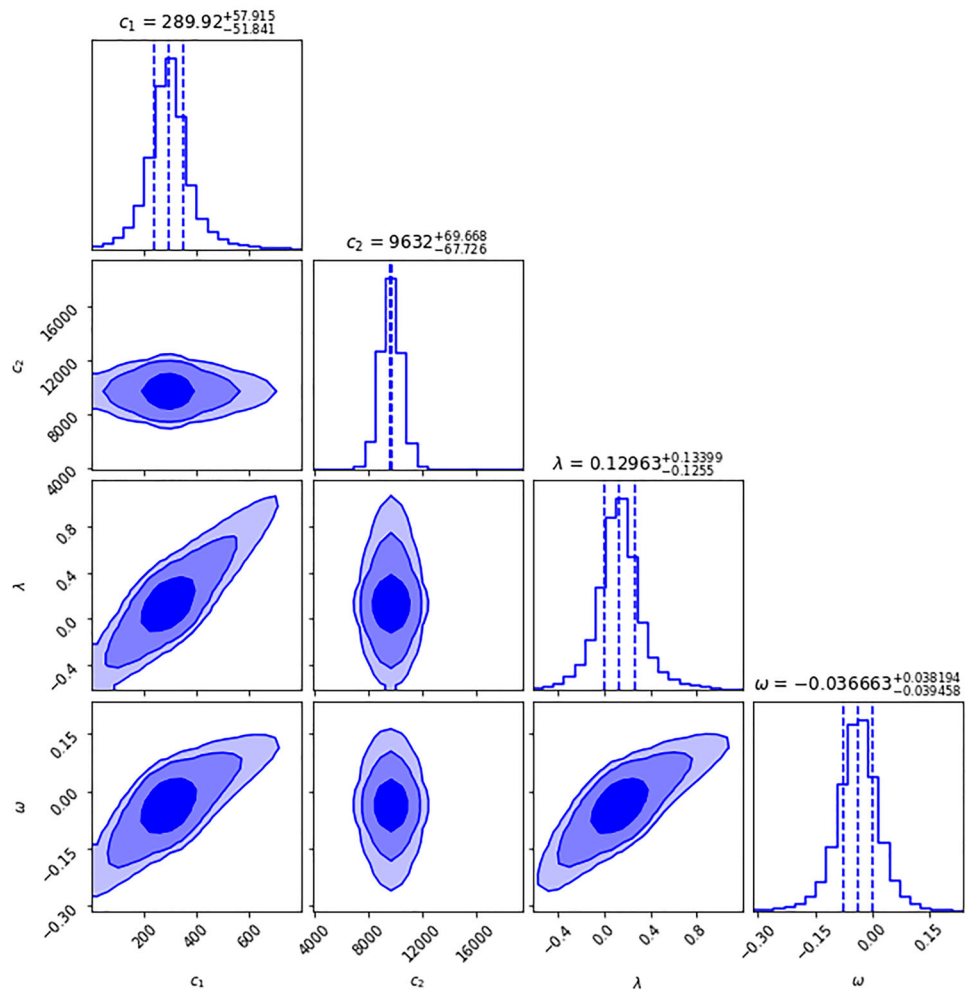
Fig. 1 The contour plot of H_0, Ω_{m0} at $1-\sigma, 2-\sigma$ and $3-\sigma$ confidence level in MCMC analysis of $H(z)$ datasets for Λ CDM model

Table 2 The MCMC results in $H(z)$ datasets analysis

Model	Parameter	Prior	Value
Λ CDM	H_0	(50, 100)	$68.0^{+2.110}_{-2.137}$
	Ω_{m0}	(0, 1)	$0.322^{+0.04403}_{-0.03846}$
	χ^2_{min}	-	26.3066
	c_1	(0, 800)	$289.92^{+57.915}_{-51.841}$
	c_2	(2000, 20000)	$9632^{+69.668}_{-67.726}$
$f(R, \bar{T})$	λ	(-1, 1.2)	$0.12963^{+0.13399}_{-0.1255}$
	ω	(-1, 1)	$-0.036663^{+0.038194}_{-0.039458}$
	χ^2_{min}	-	22.8994

for $F(R, \bar{T})$ -model with $H(z)$ datasets is shown in Fig. 3. As indicated in Table 2, we have selected a broad range of priors for our study in order to estimate the cosmological parameters, which have the highest likelihood of existing for the theoretical values of these parameters for the best-fit model. We have estimated best fit values of $c_1 = 289.92^{+57.915}_{-51.841}$, $c_2 = 9632^{+69.668}_{-67.726}$, $\lambda = 0.12963^{+0.13399}_{-0.1255}$ and $\omega = -0.036663^{+0.038194}_{-0.039458}$ at $1-\sigma, 2-\sigma$ and $3-\sigma$ errors using the priors (0, 800), (2000, 20000), (-1, 1.2) and (-1, 1), respectively. We have estimated the Hubble constant as $H_0 = 64.3627^{+1.3291}_{-1.3408}$ km s⁻¹ Mpc⁻¹ for the best fit model. Recently, Cao and Ratra [83] have obtained the value of Hubble constant $H_0 = 69.8 \pm 1.3$ km s⁻¹ Mpc⁻¹ while in [84] they estimated this value as $H_0 = 69.7 \pm 1.2$ km s⁻¹ Mpc⁻¹. Recently, Alberto Domínguez et al. [85] have obtained this parameter in their likelihood analysis of wide observational

Fig. 2 The contour plots of $c_1, c_2, \lambda, \omega$ at $1 - \sigma, 2 - \sigma$ and $3 - \sigma$ confidence level in MCMC analysis of $H(z)$ datasets



datasets as $H_0 = 66.6 \pm 1.6 \text{ km s}^{-1} \text{ Mpc}^{-1}$ and [86,87] have obtained as $H_0 = 65.8 \pm 3.4 \text{ km s}^{-1} \text{ Mpc}^{-1}$. Freedman et al. [88] have estimated the present value of Hubble constant $H_0 = 69.6 \pm 0.8 \text{ km s}^{-1} \text{ Mpc}^{-1}$, Birrer et al. [89] have measured $H_0 = 67.4^{+4.1}_{-3.2} \text{ km s}^{-1} \text{ Mpc}^{-1}$, Boruah et al. [90] have measured $H_0 = 69^{+2.9}_{-2.8} \text{ km s}^{-1} \text{ Mpc}^{-1}$ and most recently, Freedman [91] has estimated $H_0 = 69.8 \pm 0.6 \text{ km s}^{-1} \text{ Mpc}^{-1}$ and Qin Wu et al. [92] have measured $H_0 = 68.81^{+4.99}_{-4.33} \text{ km s}^{-1} \text{ Mpc}^{-1}$. Recently, in 2018 [93], the Planck Collaboration estimated that the Hubble constant is currently $H_0 = 67.4 \pm 0.5 \text{ km s}^{-1} \text{ Mpc}^{-1}$, while Riess et al. [94] obtained $H_0 = 73.2 \pm 1.3 \text{ km s}^{-1} \text{ Mpc}^{-1}$ in 2021. In comparison of the above results, the result obtained in our model for H_0 is compatible with observational datasets.

4.2 Apparent magnitude $m(z)$

The relationship between luminosity distance and redshift is one of the main observational techniques used to track the universe's evolution. The expansion of the cosmos and the redshift of the light from distant brilliant objects are taken into consideration when calculating the luminosity distance

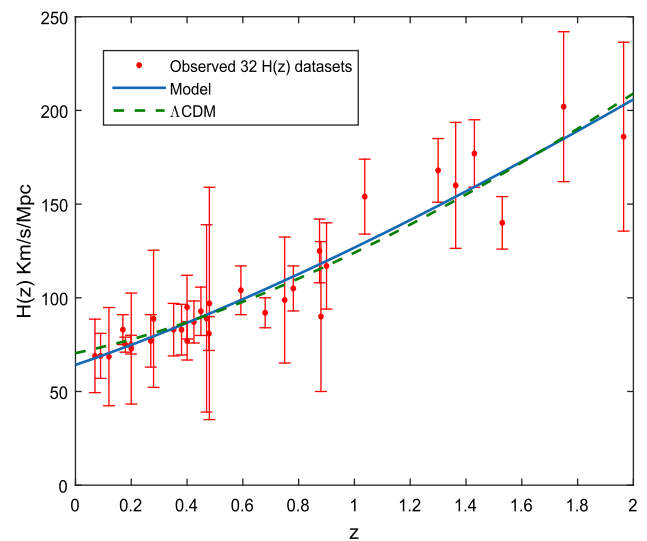


Fig. 3 The best fit shape of Hubble parameter $H(z)$ over z for our model and Λ CDM model with observed non-correlated $H(z)$ datasets

(D_L) in terms of the cosmic redshift (z). It is provided as

$$D_L = a_0 r (1 + z), \tag{31}$$

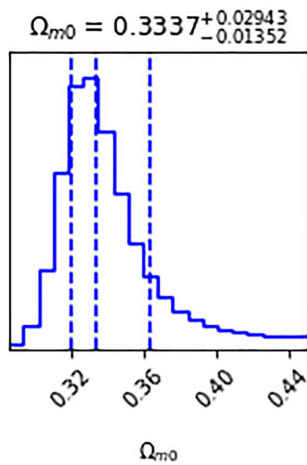


Fig. 4 The MCMC analysis of the Pantheon SNe Ia samples for Λ CDM model

where the radial coordinate of the source r , is established by

$$r = \int_0^r dr = \int_0^t \frac{cdt}{a(t)} = \frac{1}{a_0} \int_0^z \frac{cdz}{H(z)}, \tag{32}$$

where we have used $dt = dz/\dot{z}$, $\dot{z} = -H(1+z)$.

As a result, the luminosity distance is calculated as follows:

$$D_L = c(1+z) \int_0^z \frac{dz}{H(z)}. \tag{33}$$

Hence, the apparent magnitude $m(z)$ of a supernova is defined as:

$$m(z) = 16.08 + 5 \log_{10} \left[\frac{(1+z)H_0}{0.026} \int_0^z \frac{dz}{H(z)} \right]. \tag{34}$$

We use the most recent collection of 1048 datasets of the Pantheon SNe Ia samples in the $(0.01 \leq z \leq 1.7)$ range [95] in our MCMC analysis. We have used the following χ^2 formula to constrain different model parameters:

$$\chi^2(c_1, c_2, \lambda, \omega, H_0) = \sum_{i=1}^{i=N} \frac{[(m_{ob})_i - (m_{th})_i]^2}{\sigma_i^2}.$$

The entire amount of data is denoted by N , the observed and theoretical datasets of $m(z)$ are represented by m_{ob} and m_{th} , respectively, and standard deviations are denoted by σ_i .

The mathematical expression for apparent magnitude $m(z)$ is represented in Eq. (34). Figure 4 depicts the likelihood analysis of Pantheon SNe Ia datasets for Λ CDM model and the best fit values of Ω_{m0} are mentioned in Table 3. We have found the best fitted value of $\Omega_{m0} = 0.3337^{+0.02943}_{-0.01352}$ at minimum χ^2 value with $1 - \sigma$, $2 - \sigma$ and $3 - \sigma$ errors at 68%, 95% and 99% confidence level, respectively. Figure 5 shows the contour plots for $c_1, c_2, \lambda, \omega, H_0$ in MCMC analysis of Pantheon SNe Ia datasets. Figure 6 depicts the best fit curve of apparent magnitude versus z for Pantheon SNe Ia datasets for the best fit values

Table 3 The MCMC results in Pantheon SNe Ia datasets analysis

Model	Parameter	Prior	Value
Λ CDM	Ω_{m0}	(0, 1)	$0.3337^{+0.02943}_{-0.01352}$
	χ^2_{min}	–	1117.4328
	c_1	(0, 500)	$294.8^{+0.1279}_{-0.1282}$
	c_2	(1000, 10000)	$9625^{+0.1286}_{-0.1281}$
$f(R, \bar{T})$	λ	(–1, 2)	$0.2486^{+0.1090}_{-0.1596}$
	ω	(–1, 1)	$0.01065^{+0.1528}_{-0.1128}$
	H_0	(50, 100)	$67.87^{+0.1281}_{-0.1290}$
	χ^2_{min}	–	1103.6114

of model parameters. We have applied a wide range priors (0, 500), (1000, 10000), (–1, 2), (–1, 1), (50, 100) for $c_1, c_2, \lambda, \omega, H_0$, respectively, in our analysis and obtained the best fit values as $c_1 = 294.8^{+0.1279}_{-0.1282}$, $c_2 = 9625^{+0.1286}_{-0.1281}$, $\lambda = 0.2486^{+0.1090}_{-0.1596}$, $\omega = 0.01065^{+0.1528}_{-0.1128}$, $H_0 = 67.87^{+0.1281}_{-0.1290}$ with $1 - \sigma$, $2 - \sigma$ and $3 - \sigma$ errors at 68%, 95% and 99% confidence level, respectively (see Table 3). Our result is compatible with the recent observational datasets.

5 Result analysis and discussion

In this section, first we introduce matter energy density parameter Ω_m and effective dark energy density parameter Ω_{MG} , respectively as

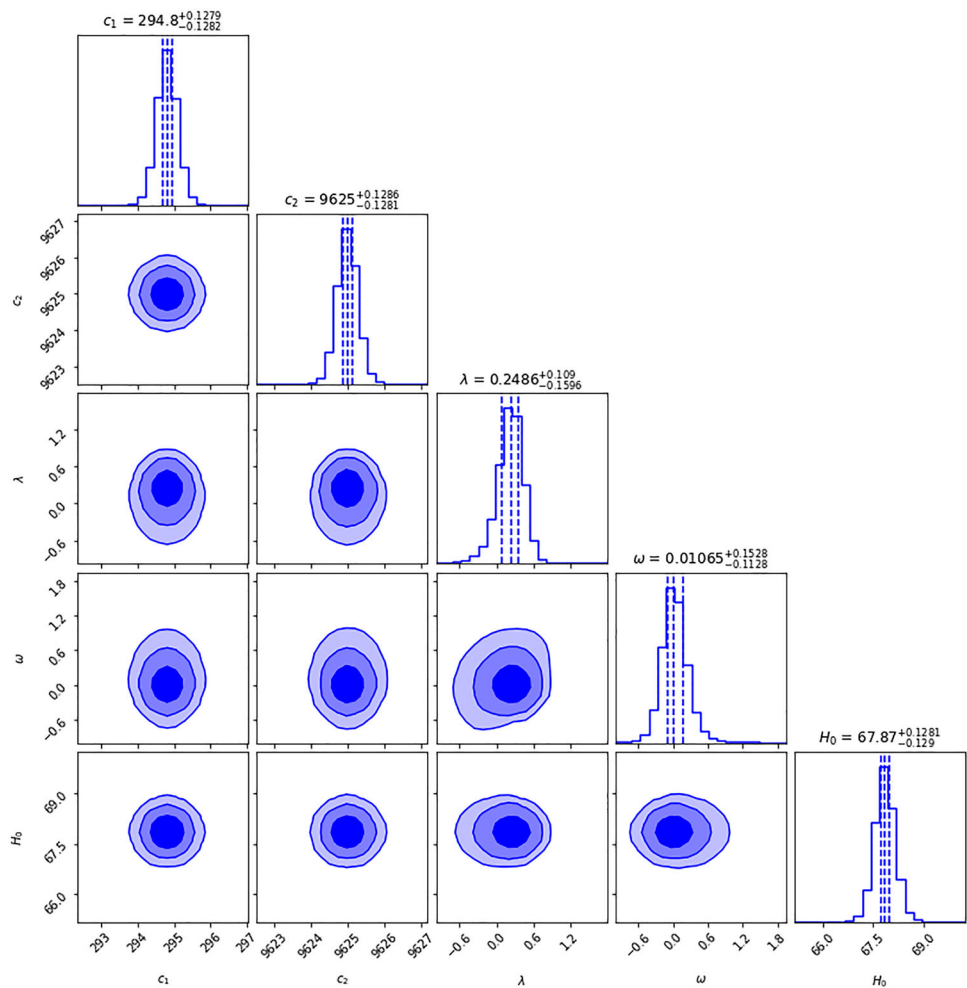
$$\Omega_m = \frac{\rho}{3(1+\lambda)H^2}, \quad \Omega_{MG} = \frac{c_1}{6(1+\lambda)H}. \tag{35}$$

From Eq. (19), we can define the relationship between energy density parameters Ω_m and Ω_{MG} as

$$\Omega_m + \Omega_{MG} = 1. \tag{36}$$

Equation (35) represents the expressions for matter energy density parameter Ω_m and effective dark energy density parameter Ω_{MG} , respectively. The geometrical evolution of Ω_m, Ω_{MG} , respectively are shown in Fig. 7a, b. Figure 7a depicts that the early universe is matter dominated $\lim_{z \rightarrow \infty} \Omega_m \rightarrow 1$ and in late-time universe $\lim_{z \rightarrow -1} \Omega_m \rightarrow 0$. Figure 7b depicts that late-time universe is dark energy dominated $\lim_{z \rightarrow -1} \Omega_{MG} \rightarrow 1$ and in early time universe $\lim_{z \rightarrow \infty} \Omega_{MG} \rightarrow 0$. At present $z=0$, we have estimated values of these parameters as $(\Omega_{m0}, \Omega_{MG0}) = (0.3767^{+0.0620}_{-0.0559}, 0.6233^{+0.0016}_{-0.0018})$, $(0.2831^{+0.0294}_{-0.0156}, 0.7169^{+0.0020}_{-0.0041})$, respectively, along two observational datasets $H(z)$ and Pantheon SNe Ia datasets while for the standard Λ CDM model, these quantities are obtained as $\Omega_{m0} = 0.322^{+0.04403}_{-0.03846}, 0.3337^{+0.02943}_{-0.01352}$ with Hubble constant $H_0 = 68.0^{+2.110}_{-2.137} \text{ km s}^{-1} \text{ Mpc}^{-1}$. These values are compatible with recent observations [83–

Fig. 5 The contour plots of $c_1, c_2, \lambda, \omega, H_0$ in MCMC analysis of the Pantheon SNe Ia samples



88]. The good observations in our model are the effective dark energy term that comes from the geometrical corrections.

The effective dark energy equation of state parameter ω_{de} is obtained as

$$\omega_{de} = -1 + \frac{1+z}{3} \frac{H'}{H} - \frac{2\lambda(1+z)H'}{c_1 - 6\lambda H}, \tag{37}$$

or

$$\omega_{de}(z) = -1 + \frac{12(1+\omega)c_2(1+z)^{3(1+\omega)}}{\frac{c_1^2}{1+\lambda} + 24c_2(1+z)^{3(1+\omega)} + c_1\sqrt{\left(\frac{c_1}{1+\lambda}\right)^2 + \frac{24c_2}{1+\lambda}(1+z)^{3(1+\omega)}} - \frac{6\lambda c_2(1+\omega)(1+z)^{3(1+\omega)}}{\frac{c_1(2+\lambda)}{2}\sqrt{\left(\frac{c_1}{1+\lambda}\right)^2 + \frac{24c_2}{1+\lambda}(1+z)^{3(1+\omega)}} - \frac{\lambda(1+\lambda)}{2}\left[\left(\frac{c_1}{1+\lambda}\right)^2 + \frac{24c_2}{1+\lambda}(1+z)^{3(1+\omega)}\right]}, \quad \lambda \neq -1. \tag{38}$$

The mathematical expression for effective dark energy EoS parameter ω_{de} is represented in Eq. (38) and its geometrical behaviour is shown in Fig. 8. From Fig. 8, we can see that effective dark energy EoS varies as $-1 \leq \omega_{de} \leq -0.6787$ along $H(z)$ datasets, $-1 \leq \omega_{de} \leq -0.5795$ along Pantheon

datasets and $-1 \leq \omega_{de} \leq -0.5176$ for Λ CDM model, over the redshift $-1 \leq z \leq 3$. At $z = 0$, we have measured the value of EoS $\omega_{de} = -0.7552^{+0.0079}_{-0.0109}, -0.7583^{+0.0103}_{-0.0018}$, respectively, along two observational datasets and for Λ CDM model it is estimated as $\omega_{de} = -0.85$. Also from Fig. 8, we observe that $\omega_{de} \rightarrow -1$ as $z \rightarrow -1$ (at late-time universe) for all datasets. Thus, these behaviours of effective

dark energy EoS parameter ω_{de} confirm that our model is in good agreement with observational datasets, and our derived $F(R, \tilde{T})$ model is very closed to Λ CDM standard cosmological model.

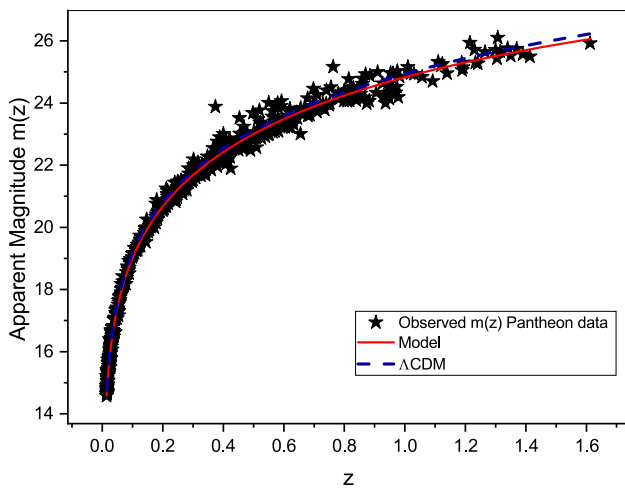


Fig. 6 The best fit plot of apparent magnitude $m(z)$ versus z for Pantheon SNe Ia samples

The expression for deceleration parameter $q(z)$ is represented in Eq. (30) and its geometrical nature is depicted in Fig. 9. From Fig. 9, we observe that $\lim_{z \rightarrow -1} q \rightarrow -1$ (accelerating phase of late-time universe) and $\lim_{z \rightarrow \infty} q \rightarrow \frac{1+3\omega}{2} > 0$ (decelerating phase of early universe) that reveals that for to obtain past decelerating universe the perfect fluid equation of state parameter should be $\omega > -\frac{1}{3}$. At present ($z = 0$) we have estimated the value of deceleration parameter $q_0 = -0.2295^{+0.0218}_{-0.0226}, -0.2590^{+0.0372}_{-0.0455}$, respectively along two observational datasets $H(z)$ and Pantheon SNe Ia and for Λ CDM standard model, it is obtained as $q_0 = -0.55$, and this reveals that the present phase of the expanding universe is accelerating which is in good agreement with recent observations. From Fig. 9, one can see that evolution of $q(z)$ shows a signature-flipping (transition) point called as transi-

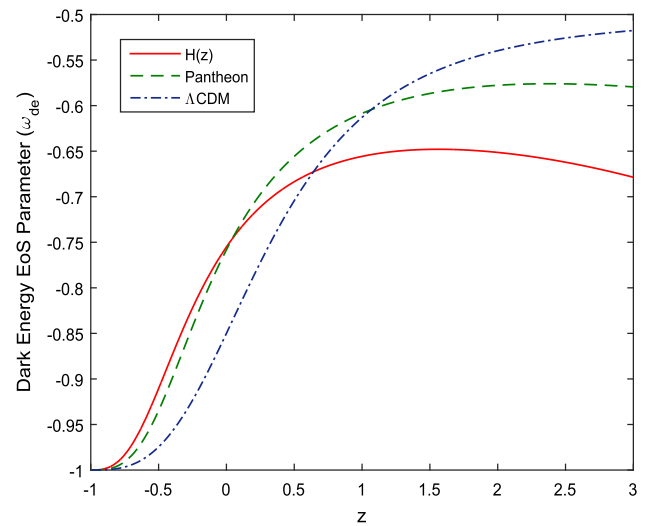


Fig. 8 The evolution of effective dark energy equation of state parameter ω_{de} versus z

tion redshift z_t at which $q = 0$ i.e., the expansion of universe is in accelerating phase for $z < z_t$ and it is in decelerating expansion phase for $z > z_t$. The general expression for z_t , we have derived from Eq. (30) as below

$$z_t = \left[\frac{c_1^2(2 + 3\omega)}{6c_2(1 + \lambda)(1 + 3\omega)} \right]^{\frac{1}{3(1+\omega)}} - 1, \quad \lambda \neq -1. \quad (39)$$

In the derived model, we have measured the transition redshift as $z_t = 0.4438^{+0.1008}_{-0.790}, 0.3651^{+0.1644}_{-0.0904}$, respectively, for two observational datasets $H(z)$ and Pantheon SNe Ia, while for standard Λ CDM model, it is obtained as $z_t = 0.671$. From Eq. (34), we can obtain ever accelerating universe for $\omega \rightarrow -1$ as $z_t \rightarrow \infty$. Recently in 2013, Farooq and Ratra [96] have measured this decelerating-accelerating

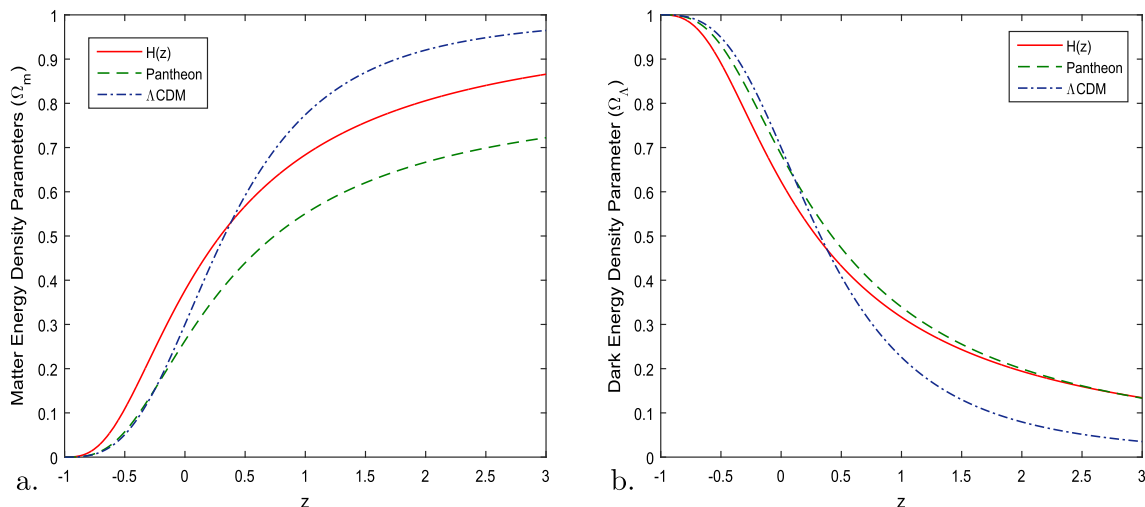


Fig. 7 The geometrical evolution of matter energy density parameter Ω_m and effective dark energy density parameter $\Omega_{MG} = \Omega_\Lambda$ over z , respectively

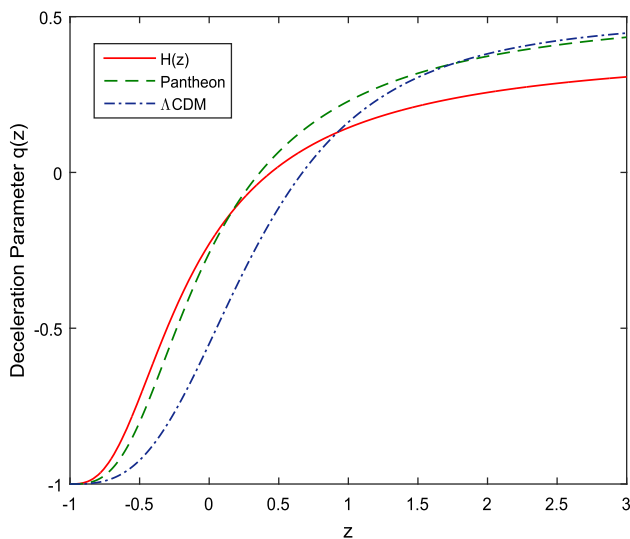


Fig. 9 The geometrical evolution of deceleration parameter $q(z)$ versus z

transition redshifts $z_t = 0.74 \pm 0.05$ while Farooq et al. [97] have estimated as $z_t = 0.74 \pm 0.04$. In 2016, Farooq et al. [98] have measured this transition redshifts $z_t = 0.72 \pm 0.05$ and in 2018, Yu et al. [99] have suggested this transition redshifts varies over $0.33 < z_t < 1.0$. Thus, the decelerating-accelerating transition redshift $z_t = 0.4438^{+0.1008}_{-0.790}, 0.3651^{+0.1644}_{-0.0904}$ measured in our model is in good agreement with the results obtained in [96–101].

5.1 Om diagnostic analysis

It is simpler to classify concepts related to cosmic dark energy because of the behavior of Om diagnostic function [102]. For a spatially homogeneous universe, the Om diagnostic function is given as

$$Om(z) = \frac{\left(\frac{H(z)}{H_0}\right)^2 - 1}{(1+z)^3 - 1}, \quad z \neq 0 \tag{40}$$

where H_0 denotes the current value of the Hubble parameter $H(z)$ as stated in Eq. (29). A negative slope of $Om(z)$ indicates quintessence motion, whereas a positive slope denotes phantom motion. The Λ CDM model is represented by the constant $Om(z)$.

Using Eq. (29) in (40), we get

$$Om(z) = \frac{\left(\left[\frac{c_1}{12(1+\lambda)} + \frac{1}{12}\sqrt{\left(\frac{c_1}{1+\lambda}\right)^2 + \left(\frac{24c_2}{1+\lambda}\right)(1+z)^{3(1+\omega)}}\right]/H_0\right)^2 - 1}{(1+z)^3 - 1}, \tag{41}$$

$z \neq 0, \lambda \neq -1.$

The mathematical expression for $Om(z)$ function is represented in Eq. (41) and its geometrical behaviour is shown in Fig. 10. From Fig. 10, we observe that the slopes are negative along the both datasets $H(z)$ datasets and Pantheon

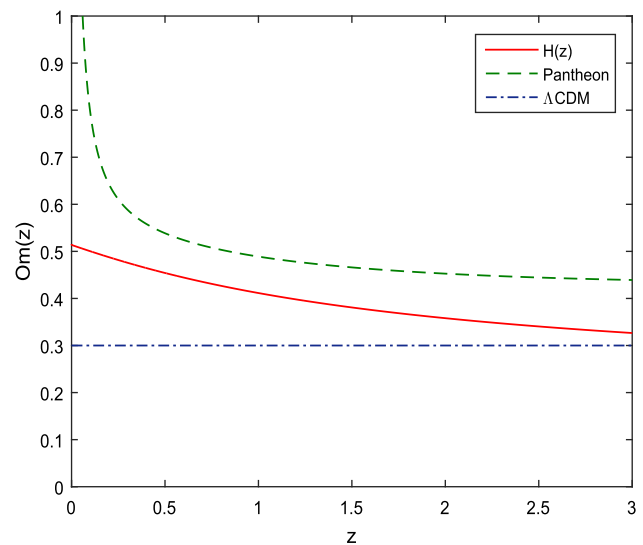


Fig. 10 Evolution of $Om(z)$ parameter versus z

SNe Ia datasets, during evolution of the universe and hence, our model behaves just like quintessence dark energy model. At late-time $\lim_{z \rightarrow -1} Om(z) \rightarrow \left[1 - \frac{c_1^2}{36(1+\lambda)^2 H_0^2}\right]$ which is a constant and it indicates that our model tends to Λ CDM model in late-time scenario.

5.2 Age of the universe

We define the age of the universe as

$$t_0 - t = \int_0^z \frac{dz}{(1+z)H(z)}, \quad z \geq 0 \tag{42}$$

where $H(z)$ is given by Eq. (29). Using this in (42), we have

$$(t_0 - t) = \lim_{z \rightarrow \infty} \int_0^z \frac{dz}{(1+z) \left[\frac{c_1}{12(1+\lambda)} + \frac{1}{12}\sqrt{\left(\frac{c_1}{1+\lambda}\right)^2 + \left(\frac{24c_2}{1+\lambda}\right)(1+z)^{3(1+\omega)}} \right]}, \tag{43}$$

$\lambda \neq -1.$

We can see that as $z \rightarrow \infty$, $(t_0 - t)$ tends to a constant value that represents the cosmic age of the universe, $(t_0 - t) \rightarrow t_0 = 0.0141602^{+0.0001027}_{-0.0000655}, 0.0122838^{+0.0006345}_{-0.0002805}$, respectively, along two datasets $H(z)$ and Pantheon SNe Ia. The present cosmic age of the universe, we have measured as $t_0 = 13.8486^{+0.1005}_{-0.0640}, 12.0135^{+0.6206}_{-0.2743}$ Gyrs, respectively along two observational datasets, which are very closed to observational estimated values and estimated Λ CDM value $t_0 = 13.3895^{+0.1240}_{-0.1129}$ Gyrs. Recently [103, 104] have measured present age of the universe as $t_0 \approx 13.87$ Gyrs.

Table 4 Information criteria for $H(z)$ datasets analysis

Model	AIC	BIC
Λ CDM	30.7203	33.2380
$F(R, \bar{T})$	32.3808	36.7623
Δ AIC	1.6605	–
Δ BIC	–	3.5243

Table 5 Information criteria for Pantheon SNe Ia datasets analysis

Model	AIC	BIC
Λ CDM	1114.4366	1124.3874
$F(R, \bar{T})$	1117.6689	1138.3845
Δ AIC	1.7677	–
Δ BIC	–	13.9970

5.3 Information criteria

It is critical to understand information criteria (IC) in order to assess a model’s level of reliability. One often used tool for this work is the Akaike Information Criterion (AIC) [105–109]. When we utilize more data, AIC provides a reasonable approximation of the divergence between a model’s predictions and reality. The Bayesian Information Criterion (BIC) [110–112] is another factor that restricts complex models more. These AIC and BIC criteria are interpreted as [113]

$$AIC = \chi_{min}^2 + \frac{2Nn}{N - n - 1}, \quad BIC = \chi_{min}^2 + n \ln N \quad (44)$$

For both scenarios, n represents the count of independent fitting parameters, whereas N represents the number of data points utilized in the analysis. In order to assess the efficacy of a dynamical dark energy (DE) model in comparison to the Λ CDM model in accurately characterizing the entire dataset, we calculate the pairwise differences Δ AIC and Δ BIC with regards to the model. The greater these disparities, the stronger the evidence against the model with a higher value of AIC (BIC)-the Λ CDM, in this instance. When the values of Δ AIC and/or Δ BIC fall between (0, 2) then confronted models are consistent to each other while their values in the range 6 and 10, it is appropriate to assert that there is “strong evidence” against the model. If the values exceed 10, it is considered “very strong evidence” [114, 115].

Tables 4 and 5 represent the scenarios of information criteria for $H(z)$ datasets and Pantheon SNe Ia datasets analysis. From Tables 4 and 5, we can see that Δ AIC = 1.6605 for $H(z)$ datasets and Δ AIC = 1.7677 for Pantheon datasets in the comparison of Λ CDM model which indicates that our derived $F(R, \bar{T})$ model is favored by datasets to be consistent with Λ CDM model while the values of Δ BIC = 3.5243 for $H(z)$ datasets which is greater than 2 and this indicates that

our derived model is less favored with Λ CDM model. From Table 5, we have Δ BIC = 13.9970 for Pantheon SNe Ia datasets which is greater than 10 that reveals that our derived model is strongly disfavored to be consistent with Λ CDM model.

6 Conclusions

We study exact cosmological models in $F(R, \bar{T})$ gravity theory in the current paper. The arbitrary function $F(R, \bar{T}) = R + \lambda\bar{T}$ has been investigated, in which R represents the Ricci-scalar curvature, \bar{T} is the torsion scalar in the context of generalized connection Γ , and λ is an arbitrary constant. After solving the field equations in a flat FLRW spacetime manifold for the Hubble parameter, we estimated the best fit values of the model parameters with $1 - \sigma$, $2 - \sigma$, and $3 - \sigma$ regions by utilizing the MCMC analysis. We have conducted a model discussion and outcome analysis using these best fit model parameter conditions. For the best fit shape of Hubble function $H(z)$, we have found the values of model parameters as $c_1 = 289.92^{+57.915}_{-51.841}$, $c_2 = 9632^{+69.668}_{-67.726}$, $\lambda = 0.12963^{+0.13399}_{-0.1255}$ and $\omega = -0.036663^{+0.038194}_{-0.039458}$ at $1 - \sigma$, $2 - \sigma$ and $3 - \sigma$ errors for $H(z)$ datasets, and $c_1 = 294.8^{+0.1279}_{-0.1282}$, $c_2 = 9625^{+0.1286}_{-0.1281}$, $\lambda = 0.2486^{+0.1090}_{-0.1596}$, $\omega = 0.01065^{+0.1528}_{-0.1128}$, $H_0 = 67.87^{+0.1281}_{-0.1290}$ with $1 - \sigma$, $2 - \sigma$ and $3 - \sigma$ errors at 68%, 95% and 99% confidence level, respectively, for Pantheon SNe Ia datasets (see Tables 2, 3). We have also find the best fit value of Hubble constant for Λ CDM model with statistically non-correlated $H(z)$ datasets as $H_0 = 68.0^{+2.110}_{-2.137}$ km s⁻¹ Mpc⁻¹. In the analysis of deceleration parameter $q(z)$, our universe model shows a transit phase dark energy model that is decelerating $q > 0$ for $z > z_t$ and accelerating $q < 0$ for $z < z_t$. We have found the transition redshift $z_t = 0.4438^{+0.1008}_{-0.790}$, $0.3651^{+0.1644}_{-0.0904}$, respectively for two observational datasets $H(z)$ and Pantheon. We have found the present value of DP as $q_0 = -0.2295^{+0.0218}_{-0.0226}$, $-0.2590^{+0.0372}_{-0.0455}$ with Hubble constant $H_0 = 64.3627^{+1.3291}_{-1.3408}$, $67.87^{+0.1281}_{-0.1290}$ km s⁻¹ Mpc⁻¹, respectively, for two datasets. The OM diagnostic analysis of $H(z)$ indicates that the current behaviour of our model is quintessential and late-time it approaches to Λ CDM model. We have found that $(\Omega_m, \Omega_{MG}) \rightarrow (0, 1)$ at late-time which is good observations for our model. We have found the present values of total energy density parameters as $(\Omega_{m0}, \Omega_{MG0}) = (0.3767^{+0.0620}_{-0.0559}, 0.6233^{+0.0016}_{-0.0018})$, $(0.2831^{+0.0294}_{-0.0156}, 0.7169^{+0.0020}_{-0.0041})$, respectively, along two observational datasets $H(z)$ and Pantheon SNe Ia datasets while for standard Λ CDM model, these quantities are as $\Omega_{m0} = 0.322^{+0.04403}_{-0.03846}$, $0.3337^{+0.02943}_{-0.01352}$ respectively along two observational datasets. We have found that the effective dark energy EoS parameter varies as $-1 \leq \omega_{de} \leq -0.6787$

along $H(z)$ datasets, $-1 \leq \omega_{de} \leq -0.5795$ along Pantheon datasets and $-1 \leq \omega_{de} \leq -0.5176$ for Λ CDM model, over the redshift $-1 \leq z \leq 3$. At $z = 0$, we have measured the value of EoS $\omega_{de} = -0.7552^{+0.0079}_{-0.0109}$, $-0.7583^{+0.0103}_{-0.0018}$, respectively, along two observational datasets and for Λ CDM model it is estimated as $\omega_{de} = -0.85$ with $\omega_{de} \rightarrow -1$ as $z \rightarrow -1$ at late-time universe. We have found the present age of the universe for our derived $F(R, \bar{T})$ model as $t_0 = 13.8486^{+0.1005}_{-0.0640}$, $12.0135^{+0.6206}_{-0.2743}$ Gyrs, respectively along two observational datasets, which are very closed to observational estimated values and estimated Λ CDM value $t_0 = 13.3895^{+0.1240}_{-0.1129}$ Gyrs. We have also, analyzed the Information Criterion AIC and BIC to compare of derived model with Λ CDM model. We have found that the $H(z)$ datasets analysis is favored our derived model to be consistent with Λ CDM model while the Pantheon datasets is less supported.

Thus, we have found that the above derived $F(R, \bar{T})$ gravity model can describe the accelerated phase of expanding universe without introducing the dark energy term Λ . The results of $F(R, \bar{T})$ gravity model is extremely very similar and closed to Λ CDM standard cosmological model but without introducing cosmological constant Λ -term. Also, we can recover the original Friedmann model without Λ -term from $F(R, \bar{T})$ gravity model by substituting $\lambda = 0$, $c_1 = 0$. This $F(R, \bar{T})$ gravity theory is the generalization of both $F(R)$ and $F(\bar{T})$ gravity theory. Thus, the present modified gravity model is interesting and attracts to researcher in this field to re-investigate it for exploring the hidden cosmological properties of this $F(R, \bar{T})$ gravity theory.

Acknowledgements This work was supported by the Ministry of Science and Higher Education of the Republic of Kazakhstan, Grant AP14870191. The authors are thankful to renowned Reviewers/Editors for their valuable suggestion to improve this manuscript.

Data Availability Statement This manuscript has no associated data. [Author's comment: Data sharing not applicable to this article as no datasets were generated or analysed during the current study].

Code Availability Statement The manuscript has no associated code/software. [Author's comment: Code/Software sharing not applicable to this article as no code/software was generated or analysed during the current study].

Declarations

Conflict of interest The author of this article has no conflict of interest. The author have no conflict of interest to declare that are relevant to the content of this article. Authors have mentioned clearly all received support from the organization for the submitted work.

Open Access This article is licensed under a Creative Commons Attribution 4.0 International License, which permits use, sharing, adaptation, distribution and reproduction in any medium or format, as long as you give appropriate credit to the original author(s) and the source, provide a link to the Creative Commons licence, and indicate if changes were made. The images or other third party material in this article

are included in the article's Creative Commons licence, unless indicated otherwise in a credit line to the material. If material is not included in the article's Creative Commons licence and your intended use is not permitted by statutory regulation or exceeds the permitted use, you will need to obtain permission directly from the copyright holder. To view a copy of this licence, visit <http://creativecommons.org/licenses/by/4.0/>.
Funded by SCOAP³.

References

1. S. Capozziello, M. De Laurentis, Extended theories of gravity. *Phys. Rep.* **509**, 167 (2011). [arXiv:1108.6266](https://arxiv.org/abs/1108.6266) [gr-qc]
2. S. Nojiri, S.D. Odintsov, Unified cosmic history in modified gravity: from $F(R)$ theory to Lorentz non-invariant models. *Phys. Rep.* **505**, 59 (2011). [arXiv:1011.0544](https://arxiv.org/abs/1011.0544) [gr-qc]
3. E.J. Copeland, M. Sami, S. Tsujikawa, Dynamics of dark energy. *Int. J. Mod. Phys. D* **15**, 1753 (2006). [arXiv:hep-th/0603057](https://arxiv.org/abs/hep-th/0603057)
4. Y.F. Cai, E.N. Saridakis, M.R. Setare, J.Q. Xia, Quintom cosmology: theoretical implications and observations. *Phys. Rep.* **493**, 1 (2010). [arXiv:0909.2776](https://arxiv.org/abs/0909.2776) [hep-th]
5. N. Bartolo, E. Komatsu, S. Matarrese, A. Riotto, Non-Gaussianity from inflation: theory and observations. *Phys. Rep.* **402**, 103 (2004). [arXiv:astro-ph/0406398](https://arxiv.org/abs/astro-ph/0406398)
6. K.S. Stelle, Renormalization of higher-derivative quantum gravity. *Phys. Rev. D* **16**, 953 (1977)
7. T. Biswas, E. Gerwick, T. Koivisto, A. Mazumdar, Towards singularity- and ghost-free theories of gravity. *Phys. Rev. Lett.* **108**, 031101 (2012). [arXiv:1110.5249](https://arxiv.org/abs/1110.5249) [gr-qc]
8. D. Lovelock, The Einstein tensor and its generalizations. *J. Math. Phys.* **12**, 498 (1971)
9. N. Deruelle, L. Farina-Busto, Lovelock gravitational field equations in cosmology. *Phys. Rev. D* **41**, 3696 (1990)
10. A. De Felice, S. Tsujikawa, $f(R)$ theories. *Living Rev. Relativ.* **13**, 3 (2010)
11. S. Nojiri, S.D. Odintsov, Modified Gauss–Bonnet theory as gravitational alternative for dark energy. *Phys. Lett. B* **631**, 1 (2005)
12. A. De Felice, S. Tsujikawa, Construction of cosmologically viable $f(G)$ gravity models. *Phys. Lett. B* **675**, 1 (2009)
13. Y.F. Cai, S. Capozziello, M. De Laurentis, E.N. Saridakis, $f(T)$ teleparallel gravity and cosmology. *Rep. Prog. Phys.* **79**, 106901 (2016). [arXiv:1511.07586](https://arxiv.org/abs/1511.07586) [gr-qc]
14. R. Ferraro, F. Fiorini, Modified teleparallel gravity: inflation without an inflation. *Phys. Rev. D* **75**, 084031 (2007). [arXiv:gr-qc/0610067](https://arxiv.org/abs/gr-qc/0610067)
15. E.V. Linder, Einstein's other gravity and the acceleration of the universe. *Phys. Rev. D* **81**, 127301 (2010). [arXiv:1005.3039](https://arxiv.org/abs/1005.3039) [astro-ph.CO]
16. G. Kofinas, E.N. Saridakis, Teleparallel equivalent of Gauss–Bonnet gravity and its modifications. *Phys. Rev. D* **90**, 084044 (2014). [arXiv:1404.2249](https://arxiv.org/abs/1404.2249) [gr-qc]
17. R. Aldrovandi, J.G. Pereira, *Teleparallel Gravity: An Introduction* (Springer, Dordrecht, 2013)
18. J.W. Maluf, The teleparallel equivalent of general relativity. *Ann. Phys.* **525**, 339 (2013)
19. A. Paliathanasis et al., Cosmological solutions of $f(T)$ gravity. *Phys. Rev. D* **94**, 023525 (2016)
20. K. Hayashi, T. Shirafuji, New general relativity. *Phys. Rev. D* **19**, 3524 (1979)
21. M. Tsamparlis, Cosmological principle and torsion. *Phys. Lett. A* **75**, 27 (1979)
22. H.I. Arcos, J.G. Pereira, Torsion gravity: a reappraisal. *Int. J. Mod. Phys. D* **13**, 2193 (2004)

23. A. Einstein, Riemannian geometry with maintaining the notion of distant parallelism. *Sitz. Preuss. Akad. Wiss.* **217**, 224 (1928). [arXiv:physics/0503046](https://arxiv.org/abs/physics/0503046), preprint
24. K. Atazadeh, F. Darabi, $f(T)$ cosmology via Noether symmetry. *Eur. Phys. J. C* **72**, 2016 (2012)
25. S. Basilakos et al., Noether symmetries and analytical solutions in cosmology: a complete study. *Phys. Rev. D* **88**, 103526 (2013)
26. M.E. Rodrigues et al., Bianchi type-*I*, type-*III* and Kantowski–Sachs solutions in $f(T)$ gravity. *Astrophys. Space Sci.* **357**, 129 (2015)
27. A. Paliathanasis et al., New Schwarzschild-like solutions in $f(T)$ gravity through Noether symmetries. *Phys. Rev. D* **89**, 104042 (2014)
28. S. Capozziello et al., Exact charged black-hole solutions in D-dimensional $f(T)$ gravity: torsion vs curvature analysis. *J. High Energy Phys.* **89**, 039 (2013)
29. Y.F. Cai et al., Matter bounce cosmology with the $f(T)$ gravity. *Class. Quantum Gravity* **28**, 215011 (2011)
30. J. de Haro, J. Amorós, Viability of the matter bounce scenario. *J. Phys. Conf. Ser.* **600**, 012024 (2015)
31. J. de Haro, J. Amorós, Matter bounce scenario in $F(T)$ gravity. *PoS FFP* **14**, 163 (2016)
32. W. El Hanafy, G.G.L. Nashed, Lorenz gauge fixing of $f(T)$ teleparallel cosmology. *Int. J. Mod. Phys. D* **26**, 1750154 (2017)
33. K. Bamba et al., Bounce inflation in $f(T)$ cosmology: a unified inflation–quintessence field. *Phys. Rev. D* **94**, 083513 (2016)
34. G.R. Bengochea, R. Ferraro, Dark torsion as the cosmic speed-up. *Phys. Rev. D* **79**, 124019 (2009)
35. K. Bamba et al., Equation of state for dark energy in $f(T)$ gravity. *J. Cosmol. Astropart. Phys.* **01**, 021 (2011)
36. R. Myrzakulov, Accelerating universe from $F(T)$ gravity. *Eur. Phys. J. C* **71**, 1752 (2011)
37. A.N. Nurbaki et al., Spherical and cylindrical solutions in $f(T)$ gravity by Noether symmetry approach. *Eur. Phys. J. C* **80**, 108 (2020)
38. K.N. Singh, Conformally symmetric traversable wormholes in modified teleparallel gravity. *Phys. Rev. D* **101**, 084012 (2020)
39. F. Hammad et al., Noether charge and black hole entropy in teleparallel gravity. *Phys. Rev. D* **100**, 124040 (2019)
40. A. Dixit, A. Pradhan, D.C. Maurya, A probe of cosmological models in modified teleparallel gravity. *Int. J. Geom. Methods Mod. Phys.* **18**, 2150208 (2023)
41. D.C. Maurya, Accelerating scenarios of viscous fluid universe in modified $f(T)$ gravity. *Int. J. Geom. Methods Mod. Phys.* **19**, 2250144 (2022)
42. A. Pradhan, A. Dixit, M. Zeyauddin, Reconstruction of Λ CDM model from $f(T)$ gravity in viscous-fluid universe with observational constraints. *Int. J. Geom. Methods Mod. Phys.* (2023). <https://doi.org/10.1142/S0219887824500270>
43. D.C. Maurya, Reconstructing Λ CDM $f(T)$ gravity model with observational constraints. *Inter. J. Geom. Methods Mod. Phys.* (2024). <https://doi.org/10.1142/S0219887824500397>
44. T. Harko, T.S. Koivisto, F.S.N. Lobo, G.J. Olmo, D. Rubiera-García, Coupling matter in modified Q gravity. *Phys. Rev. D* **98**, 084043 (2018). [arXiv:1806.10437](https://arxiv.org/abs/1806.10437) [gr-qc]
45. G.Y. Bogoslovsky, H.F. Goenner, Finslerian spaces possessing local relativistic symmetry. *Gen. Relativ. Gravit.* **31**, 1565 (1999). [arXiv:gr-qc/9904081](https://arxiv.org/abs/gr-qc/9904081)
46. N.E. Mavromatos, S. Sarkar, A. Vergou, Stringy space-time foam, Finsler-like metrics and dark matter relics. *Phys. Lett. B* **696**, 300 (2011). [arXiv:1009.2880](https://arxiv.org/abs/1009.2880) [hep-th]
47. A.P. Kouretsis, M. Stathakopoulos, P.C. Stavrinou, Covariant kinematics and gravitational bounce in Finsler space-times. *Phys. Rev. D* **86**, 124025 (2012). [arXiv:1208.1673](https://arxiv.org/abs/1208.1673) [gr-qc]
48. S. Basilakos, A.P. Kouretsis, E.N. Saridakis, P. Stavrinou, Resembling dark energy and modified gravity with Finsler–Randers cosmology. *Phys. Rev. D* **88**, 123510 (2013). [arXiv:1311.5915](https://arxiv.org/abs/1311.5915) [gr-qc]
49. A. Triantafyllopoulos, P.C. Stavrinou, Weak field equations and generalized FRW cosmology on the tangent Lorentz bundle. *Class. Quantum Gravity* **35**, 085011 (2018)
50. S. Ikeda, E.N. Saridakis, P.C. Stavrinou, A. Triantafyllopoulos, Cosmology of Lorentz fiber-bundle induced scalar-tensor theories. *Phys. Rev. D* **100**, 124035 (2019). [arXiv:1907.10950](https://arxiv.org/abs/1907.10950) [gr-qc]
51. G. Minas, E.N. Saridakis, P.C. Stavrinou, A. Triantafyllopoulos, Bounce cosmology in generalized modified gravities. *Universe* **5**, 74 (2019). [arXiv:1902.06558](https://arxiv.org/abs/1902.06558) [gr-qc]
52. F.W. Hehl, J.D. McCrea, E.W. Mielke, Y. Ne’eman, identities, Metric-affine gauge theory of gravity: field equations, Noether identities, world spinors, and breaking of dilation invariance. *Phys. Rep.* **258**, 1 (1995). [arXiv:gr-qc/9402012](https://arxiv.org/abs/gr-qc/9402012)
53. J. Beltran Jimenez, A. Golovnev, M. Karciauskas, T.S. Koivisto, Bimetric variational principle for general relativity. *Phys. Rev. D* **86**, 084024 (2012). [arXiv:1201.4018](https://arxiv.org/abs/1201.4018) [gr-qc]
54. N. Tamanini, Variational approach to gravitational theories with two independent connections. *Phys. Rev. D* **86**, 024004 (2012). [arXiv:1205.2511](https://arxiv.org/abs/1205.2511) [gr-qc]
55. A. Singh, A. Pradhan, A. Beesham, Cosmological aspects of anisotropic chameleonic Brans–Dicke gravity. *New Astron.* **100**, 101995 (2023)
56. R. Myrzakulov, FRW cosmology in $F(R, T)$ gravity. *Eur. Phys. J. C* **72**, 2203 (2012). [arXiv:1207.1039](https://arxiv.org/abs/1207.1039) [gr-qc]
57. T. Harko, F.S.N. Lobo, S. Nojiri, S.D. Odintsov, $f(R, T)$ gravity. *Phys. Rev. D* **84**, 024020 (2011). [arXiv:1104.2669](https://arxiv.org/abs/1104.2669) [gr-qc]
58. A. Conroy, T. Koivisto, The spectrum of symmetric teleparallel gravity. *Eur. Phys. J. C* **78**, 923 (2018). [arXiv:1710.05708](https://arxiv.org/abs/1710.05708) [gr-qc]
59. M. Sharif, S. Rani, R. Myrzakulov, Analysis of $F(R, T)$ gravity models through energy conditions. *Eur. Phys. J. Plus* **128**, 123 (2013). [arXiv:1210.2714](https://arxiv.org/abs/1210.2714) [gr-qc]
60. M. Jamil, D. Momeni, M. Raza, R. Myrzakulov, Reconstruction of some cosmological models in $f(R, T)$ cosmology. *Eur. Phys. J. C* **72**, 1999 (2012)
61. S. Capozziello, M. De Laurentis, R. Myrzakulov, Noether symmetry approach for teleparallel-curvature cosmology. *Int. J. Geom. Methods Mod. Phys.* **12**, 1550095 (2015). [arXiv:1412.1471](https://arxiv.org/abs/1412.1471) [gr-qc]
62. P. Feola, X.J. Forteza, S. Capozziello, R. Cianci, S. Vignolo, Mass-radius relation for neutron stars in $f(R) = R + \alpha R^2$ gravity: a comparison between purely metric and torsion formulations. *Phys. Rev. D* **101**, 044037 (2020). [arXiv:1909.08847](https://arxiv.org/abs/1909.08847) [astro-ph.HE]
63. E.N. Saridakis, S. Myrzakulov, K. Myrzakulov, K. Yerzhanov, Cosmological applications of Myrzakulov gravity. *Phys. Rev. D* **102**, 023525 (2020). [arXiv:1912.03882](https://arxiv.org/abs/1912.03882) [gr-qc]
64. F.K. Anagnostopoulos, S. Basilakos, E.N. Saridakis, Observational constraints on Myrzakulov gravity. *Phys. Rev. D* **103**, 104013 (2021). [arXiv:2012.06524](https://arxiv.org/abs/2012.06524)
65. N. Myrzakulov, R. Myrzakulov, L. Ravera, Metric-affine Myrzakulov gravity theories. *Symmetry* **13**, 1855 (2021). [arXiv:2108.00957](https://arxiv.org/abs/2108.00957)
66. D. Iosifidis, N. Myrzakulov, R. Myrzakulov, Metric-affine version of Myrzakulov $F(R, T, Q, T)$ gravity and cosmological applications. *Universe* **7**, 262 (2021). [arXiv:2106.05083](https://arxiv.org/abs/2106.05083)
67. T. Harko, N. Myrzakulov, R. Myrzakulov, S. Shahidi, Non-minimal geometry-matter couplings in Weyl–Cartan space-times: Myrzakulov $F(R, T, Q, T_m)$ gravity (2021). [arXiv:2110.00358v1](https://arxiv.org/abs/2110.00358v1)
68. R. Saleem, A. Saleem, Variable constraints on some Myrzakulov models to study Baryon asymmetry. *Chin. J. Phys.* **84**, 471–485 (2023)
69. D. Iosifidis, R. Myrzakulov, L. Ravera, G. Yergaliyeva, K. Yerzhanov, Metric-affine vector–tensor correspondence and

- implications in $F(R, T, Q, T, D)$ Gravity. *Phys. Dark Univ.* **37**, 101094 (2022). [\[arXiv:2111.14214\]](#)
70. G. Papagiannopoulos, S. Basilakos, E.N. Saridakis, Dynamical system analysis of Myrzakulov gravity. *Phys. Rev. D* **106**, 103512 (2022). [arXiv:2202.10871](#)
 71. S. Kazempour, A.R. Akbarieh, Cosmological study in $F(R, T)$ quasi-dilaton massive gravity. (2023). [arXiv:2309.09230](#)
 72. R. Myrzakulov, Dark energy in $F(R, T)$ gravity. (2021). [arXiv:1205.5266v6](#) [physics.gen-ph]
 73. R. Myrzakulov, Gravity and k -essence. *Gen. Relativ. Gravit.* **44**, 3059–3080 (2012). [arXiv:1008.4486](#) [astro-ph.CO]
 74. D.W. Hogg, D.F. Mackey, Data analysis recipes: using Markov chain Monte Carlo. *Astrophys. J. Suppl. Ser.* **236**, 18 (2018). [arXiv:1710.06068](#) [astro-ph.IM]
 75. C. Zhang et al., Four new observational $H(z)$ data from luminous red galaxies in the Sloan Digital Sky Survey data release seven. *Res. Astron. Astrophys.* **14**, 1221 (2014)
 76. J. Simon et al., Constraints on the redshift dependence of the dark energy potential. *Phys. Rev. D* **71**, 123001 (2005)
 77. M. Moresco et al., Improved constraints on the expansion rate of the Universe up to $z \sim 1.1$ from the spectroscopic evolution of cosmic chronometers. *J. Cosmol. Astropart. Phys.* **8**, 006 (2012)
 78. M. Moresco et al., A 6% measurement of the Hubble parameter at $z \sim 0.45$: direct evidence of the epoch of cosmic re-acceleration. *J. Cosmol. Astropart. Phys.* **5**, 014 (2016)
 79. A.L. Ratsimbazafy et al., Age-dating luminous red galaxies observed with the Southern African Large Telescope. *MNRAS* **467**, 3239 (2017)
 80. D. Stern et al., Cosmic chronometers: constraining the equation of state of dark energy. I: $H(z)$ measurements. *J. Cosmol. Astropart. Phys.* **2**, 008 (2010)
 81. N. Borghi et al., Toward a better understanding of cosmic chronometers: a new measurement of $H(z)$ at $z \sim 0.7$. *Astrophys. J. Lett.* **928**, L4 (2022)
 82. M. Moresco, Raising the bar: new constraints on the Hubble parameter with cosmic chronometers at $z \sim 2$. *MNRAS* **450**, L16 (2015)
 83. S. Cao, B. Ratra, $H_0 = 69.8 \pm 1.3 \text{ km s}^{-1} \text{ Mpc}^{-1}$, $\Omega_{m0} = 0.288 \pm 0.017$, and other constraints from lower-redshift, non-CMB, expansion-rate data. *Phys. Rev. D* **107**, 103521 (2023). [arXiv:2302.14203](#) [astro-ph.CO]
 84. S. Cao, B. Ratra, Using lower-redshift, non-CMB, data to constrain the Hubble constant and other cosmological parameters. *MNRAS* **513**, 5686–5700 (2022). [arXiv:2203.10825](#) [astro-ph.CO]
 85. A. Domínguez et al., A new measurement of the Hubble constant and matter content of the Universe using extra-galactic background light γ -ray attenuation. (2019). [arXiv:1903.12097v2](#) [astro-ph.CO]
 86. Chan-Gyung. Park, Bharat Ratra, Using SPTpol, Planck 2015, and non-CMB data to constrain tilted spatially-flat and untilted non-flat Λ CDM, XCDM, and ϕ CDM dark energy inflation cosmologies. *Phys. Rev. D* **101**, 083508 (2020). [arXiv:1908.08477](#) [astro-ph.CO]
 87. W. Lin, M. Ishak, A Bayesian interpretation of inconsistency measures in cosmology. *JCAP* **2105**, 009 (2021). [arXiv:1909.10991v3](#) [astro-ph.CO]
 88. W.L. Freedman et al., Calibration of the Tip of the Red Giant Branch (TRGB) (2020). [arXiv:2002.01550v1](#) [astro-ph.GA]
 89. S. Birrer et al., TDCOSMO IV: hierarchical time-delay cosmography—joint inference of the hubble constant and galaxy density profiles. *A&A* **643**, A165 (2020). [arXiv:2007.02941v3](#) [astro-ph.CO]
 90. S.S. Boruah, M.J. Hudson, G. Lavaux, Peculiar velocities in the local Universe: comparison of different models and the implications for H_0 and dark matter. (2020). [arXiv:2010.01119v1](#) [astro-ph.CO]
 91. L. Wendy, *Measurements of the Hubble Constant: Tensions in Perspective* (Freedman, Washington, 2021). [arXiv:2106.15656v1](#) [astro-ph.CO]
 92. Q. Wu, G.Q. Zhang, F.Y. Wang, An 8% determination of the Hubble constant from localized fast radio bursts. (2022). [arXiv:2108.00581v2](#) [astro-ph.CO]
 93. Planck Collaboration, N. Aghanim, Y. Akrami et al., Planck 2018 results. VI. Cosmological parameters. *A&A* **641**, A6 (2020). <https://doi.org/10.1051/0004-6361/201833910>. [\[arXiv:1807.06209\]](#) [astro-ph.CO]
 94. A.G. Riess, S. Casertano, W. Yuan et al., Cosmic distances calibrated to 1% precision with Gaia EDR3 parallaxes and Hubble Space Telescope photometry of 75 Milky Way Cepheids Confirm Tension with Λ CDM. *ApJ* **908**(1), L6 (2021). <https://doi.org/10.3847/20418213/abdbaf>. [arXiv:2012.08534](#)
 95. D.M. Scolnic et al., The complete light-curve sample of spectroscopically confirmed SNe Ia from Pan-STARRS1 and cosmological constraints from the combined pantheon sample. *Astrophys. J.* **859**, 101 (2018)
 96. O. Farooq, B. Ratra, Hubble parameter measurement constraints on the cosmological deceleration-acceleration transition redshift. (2013). [arXiv:1301.5243v1](#) [astro-ph.CO]
 97. O. Farooq, S. Crandall, B. Ratra, Binned Hubble parameter measurements and the cosmological deceleration-acceleration transition. (2013). [arXiv:1305.1957v1](#) [astro-ph.CO]
 98. O. Farooq, F. Madiyar, S. Crandall, B. Ratra, Hubble parameter measurement constraints on the redshift of the deceleration-acceleration transition, dynamical dark energy, and space curvature. (2016). [arXiv:1607.03537v2](#) [astro-ph.CO]
 99. H. Yu, B. Ratra, F.-Y. Wang, Hubble parameter and baryon acoustic oscillation measurement constraints on the Hubble constant, the deviation from the spatially-flat Λ cdm model, the deceleration-acceleration transition redshift, and spatial curvature. (2018). [arXiv:1711.03437v2](#) [astro-ph.CO]
 100. Mohit K. Sharma et al., Observational constraints on the massive neutrinos induced late-time cosmic acceleration. *Phys. Scr.* **97**, 085010 (2022). [arXiv:2108.08913](#) [hep-ph]
 101. Mohit K. Sharma et al., The oscillatory universe, phantom crossing and the Hubble tension. *Ann. Phys.* **454**, 169345 (2023). [arXiv:2205.13514](#) [gr-qc]
 102. V. Sahni, A. Shafieloo, A.A. Starobinsky, Two new diagnostics of dark energy. *Phys. Rev. D* **78**, 103502 (2008)
 103. A. Pradhan et al., Modeling transit dark energy in $f(R, L_m)$ -gravity. *Int. J. Geom. Methods Mod. Phys.* **20**, 2350105 (2023)
 104. D.C. Maurya, Constrained Λ CDM dark energy models in higher derivative $F(R, L_m)$ -gravity theory. *Phys. Dark Univ.* **42**, 101373 (2023). <https://doi.org/10.1016/j.dark.2023.101373>
 105. S.I. Vrieze, Model selection and psychological theory: a discussion of the differences between the Akaike Information Criterion (AIC) and the Bayesian Information Criterion (BIC). *Psychol. Methods* **17**, 228 (2012)
 106. M. Tan, R. Biswas, The reliability of the Akaike Information Criterion method in cosmological model selection. *Mon. Not. R. Astron. Soc.* **419**, 3292–3303 (2012)
 107. M. Rezaei, M. Malekjani, Comparison between different methods of model selection in cosmology. *Eur. Phys. J. Plus* **136**, 219 (2021)
 108. F. Arevalo, A. Cid, J. Moya, AIC and BIC for cosmological interacting scenarios. *Eur. Phys. J. C* **77**, 1–13 (2017)
 109. K. Tauscher, D. Rapetti, J.O. Burns, A new goodness-of-fit statistic and its application to 21-cm cosmology. *J. Cosmol. Astropart. Phys.* **2018**, 015 (2018)
 110. G. Schwarz, Estimating the dimension of a model. *Ann. Stat.* **6**, 461–464 (1978)

111. F.K. Anagnostopoulos, S. Basilakos, E.N. Saridakis, Bayesian analysis of $f(T)$ gravity using $f\sigma_8$ data. *Phys. Rev. D* **100**, 083517 (2019)
112. F.K. Anagnostopoulos, S. Basilakos, E.N. Saridakis, Observational constraints on Myrzakulov gravity. *Phys. Rev. D* **103**, 104013 (2021)
113. J. Solà et al., First evidence of running cosmic vacuum: challenging the concordance model. *Astrophys. J.* **836**, 43 (2017)
114. H. Akaike, A new look at the statistical model identification. *ITAC* **19**, 716 (1974)
115. K.P. Burnham, D.R. Anderson, *Model Selection and Multimodel Inference* (Springer, New York, 2002)